BIOCHEMISTRY
including biophysical chemistry & molecular biology

ARTICLE

pubs.acs.org/biochemistry

Arabidopsis thaliana NIP7;1: An Anther-Specific Boric Acid Transporter of the Aquaporin Superfamily Regulated by an Unusual Tyrosine in Helix 2 of the Transport Pore

Tian Li,[†] Won-Gyu Choi,[‡] Ian S. Wallace,[‡] Jerome Baudry,[†,‡,§] and Daniel M. Roberts*[,†,‡]

[†]Program in Genome Science and Technology and [‡]Department of Biochemistry and Cellular and Molecular Biology, The University of Tennessee, Knoxville, Tennessee 37996, United States

[§]UT/ORNL Center for Molecular Biophysics, Oak Ridge, Tennessee 37830, United States

Supporting Information

ABSTRACT: Plant nodulin-26 intrinsic proteins (NIPs) are members of the aquaporin superfamily that serve as multifunctional transporters of uncharged metabolites. In *Arabidopsis thaliana*, a specific NIP pore subclass, known as the NIP II proteins, is represented by *AtNIP5;1* and *AtNIP6;1*, which encode channel proteins expressed in roots and leaf nodes, respectively, that participate in the transport of the critical cell wall nutrient boric acid. Modeling of the protein encoded by the *AtNIP7;1* gene shows that it is a third member of the NIP II pore subclass in *Arabidopsis*. However, unlike AtNIP5;1 and AtNIP6;1 proteins, which form constitutive boric acid channels, AtNIP7;1 forms a channel with an extremely low intrinsic boric acid transport activity. Molecular modeling and molecular dynamics simulations of AtNIP7;1 suggest that a conserved tyrosine residue (Tyr81) located in transmembrane helix 2 adjacent to the aromatic arginine (ar/R) pore selectivity region stabilizes a closed pore conformation through interaction with the canonical Arg220 in ar/R region. Substitution of Tyr81 with a Cys residue, characteristic of established NIP boric acid channels, results in opening of the AtNIP7;1 pore that acquires a robust, transport activity for boric acid as well as other NIP II test solutes (glycerol and urea). Substitution of a Phe for Tyr81 also opens the channel, supporting the prediction from MD simulations that hydrogen bond interaction between the Tyr81 phenol group and the ar/R Arg may contribute to the stabilization of a closed pore state. Expression analyses show that *AtNIP7;1* is selectively expressed in developing anther tissues of young floral buds of *A. thaliana*, principally in developing pollen grains of stage 9−11 anthers. Because boric acid is both an essential nutrient as well as a toxic compound at high concentrations, it is proposed that Tyr81 modulates transport and may provide an additional level of regulation for this transporter in male gametophyte development.

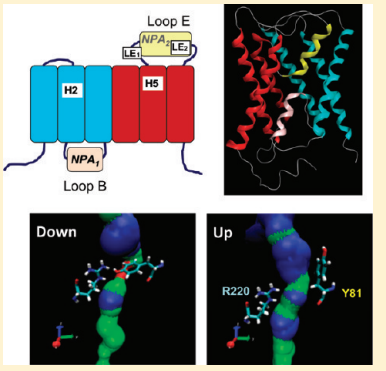

The major intrinsic protein (MIP)/aquaporin superfamily consists of integral membrane protein channels that facilitate the transport of water and other uncharged solutes across cellular membranes.[1−4] Crystallographic analyses show that MIPs share a common topology known as the "hourglass fold" (reviewed in ref 5). The hourglass fold consists of six transmembrane α-helices with two conserved loop regions (NPA boxes) that form half-helices that fold back into the membrane forming a seventh pseudotransmembrane helix. MIPs are tetrameric with each monomer containing a transport pore. Structural analyses show that the principal constriction in the pore is the aromatic arginine (ar/R) selectivity filter.[6] The ar/R region is formed by four amino acids (one each from transmembrane helices 2 and 5 and two from the second NPA half-helix) that control transport selectivity on the basis of size, hydrophobicity, and hydrogen bonding with transported substrates.

Compared to other organisms, higher plants have a larger and more diverse complement of MIP genes.[7−11] *Arabidopsis thaliana* possesses 35 MIP genes that are divided into four phylogenetic subfamilies: plasma membrane intrinsic proteins (PIPs), tonoplast intrinsic proteins (TIPs), nodulin 26-like intrinsic proteins (NIPs), and small basic intrinsic proteins (SIPs).[9,10] The NIPs make up a plant-specific family that shares homology with the archetype of the family, soybean nodulin 26. The *A. thaliana* NIP subfamily contains nine genes that encode proteins that can be segregated into two broad phylogenetic pore families, NIP I and NIP II, based on differences in the proposed ar/R selectivity region.[12] The subclass II NIPs contain a conserved ar/R "pore signature" that is composed of Ala/Gly/Thr at the helix 2 position (H2), Val/Ile at the helix 5 position (H5), and a Gly/Ala (LE_1) and an invariant Arg (LE_2) at the two loop E positions.

Analyses of two NIP II proteins, AtNIP5;1[13] and AtNIP6;1,[14] provide evidence for organ-specific roles in boron nutrition.[15] AtNIP5;1 exhibits root-specific expression that can be induced by boric acid limitation.[13] In contrast, AtNIP6;1 is expressed in a shoot-specific manner, particularly within the phloem vascular

Received: March 25, 2011
Revised: May 31, 2011
Published: June 28, 2011

tissue of stem nodes, and petioles of young developing leaves.[14] AtNIP5;1 and AtNIP6;1 T-DNA insertional mutants exhibit developmental phenotypes that are dependent upon boric acid concentration within the growth medium.[13,14] These phenotypes are manifested by an enhanced sensitivity to B deficiency that results in gross reductions in cell elongation and tissue expansion, particularly in young developing organs, and is likely the result of inadequate boric acid uptake leading to defective pectic cell wall development.[16] Analysis of the transport function of AtNIP5;1 and AtNIP6;1 in *Xenopus* oocytes showed that both proteins exhibit bidirectional $B(OH)_3$ transport activities, and it has been proposed that they serve to facilitate boric acid uptake and localization to developing tissues, particularly under conditions of boron limitation.[13,14]

In this study, we show that a third *A. thaliana* NIP II protein, AtNIP7;1, is selectively expressed in flowers within developing pollen and encodes a transporter that apparently is regulated in an unusual manner by a conserved tyrosine residue on transmembrane helix 2.

EXPERIMENTAL PROCEDURES

Homology Model and Molecular Dynamics Simulations. Alignments of the AtNIP7;1 protein sequence (TAIR: At3g06100) with aquaporin/glyceroporin template structures (AQP1, PDB entry 1J4N; AQP0, PDB entry 1YMG; AQP4, PDB entry 3GD8; AQP5, PDB entry 3D9S; GlpF, PDB entry 1LDI; AQPz, PDB entry 1RC2) were created by using MOE version 2008.10 (Molecular Operating Environment, Montreal, QC) with structural alignment enabled and the blosum62 substitution matrix. The alignment results were adjusted manually on the basis of the multiple-sequence alignment of Gorelick et al.[17] and the conserved motifs of the aquaporin fold.[18] A structural homology model of AtNIP7;1 was obtained using the homology modeling program in MOE and the CHARMM27 force field.[19] An ensemble of 10 possible structures for AtNIP7;1 was generated, with no intermediate energy minimization (to avoid artifactual "swelling" of the transmembrane region). The 10 models were subsequently ranked using MOE's packing algorithm.

The AtNIP7;1 model with the most favorable packing score (2.1313) was used for molecular dynamics simulations. The homology model was energy-minimized using the CHARMM27 force field and distance-dependent dielectric down to an energy gradient of 10^{-5} kcal mol^{-1} Å^{-2}. All α-carbons were fixed during the energy minimization, again to prevent swelling of the transmembrane region of the protein. Molecular dynamics were run at a temperature of 310 K for 5 ns, using a 1 ps integration time step in the canonical (NPT) thermodynamic ensemble. Pore diameters were calculated using HOLE[20] from selected structural snapshots from the molecular dynamics trajectory.

Protein Expression and Transport Analyses in *Xenopus* Oocytes. *Xenopus laevis* expression constructs of AtNIP7;1 were prepared in the pXβG-ev-1 vector with an in-frame N-terminal FLAG epitope tag as described in ref 21. The pXβG AtNIP7;1 construct was used as a template for PCR mutagenesis by using the QuickChange site-directed mutagenesis kit (Stratagene) and the mutagenesis primers listed in Table S1 of the Supporting Information. The PCR products were digested with the *Dpn*I enzyme, and the mixture was used to transform *Escherichia coli* DH5α. pXβG-ev-1 constructs containing AtNIP5;1[14], At NIP6;1[14] and ApAQP1 aquaporin[32] were generated as described previously. cRNA was generated from *Xba*I-linearized plasmids by in vitro transcription (AmpliCap-Max T3 High Yield Message Maker Kit, Epicenter).

Defolliculated *Xenopus* oocytes were prepared and microinjected with 46 ng of various cRNAs as previously described.[14,21] Oocytes were incubated at 16 °C for 72 h in Ringer's solution [96 mM NaCl, 2 mM KCl, 5 mM $MgCl_2$, 0.6 mM $CaCl_2$, and 5 mM HEPES-OH (pH 7.6); osmolarity = 210 mosmol/kg] with 1000 units of penicillin-streptomycin prior to the assay. Negative control oocytes were mock injected with 46 ng of RNase-free sterile water.

The osmotic water permeability (P_f) was measured at 15 °C from the rate of oocyte swelling in hypoosmotic medium containing 30% oocyte Ringer's solution (60 mOsm/kg) by video microscopy as described in ref 23. The P_f was determined by using the osmotic water permeability equation:

$$P_f = \frac{(V_0/S_0)[d(V/V_0)/dt]}{(S_{real}/S_{sphere})V_w(osm_{in} - osm_{out})}$$

where V_0 is the initial oocyte volume, S_0 is the initial oocyte surface area, osm_{in} is the osmolarity in the oocyte, osm_{out} is the osmolarity of the media, V_w is the partial molar volume of water, S_{real} is the actual surface area of the oolemma, and S_{sphere} is the area calculated by assuming a sphere. S_{real}/S_{sphere} is taken to be 9 for all measurements.

Boric acid uptake assays were performed by equilibrating oocytes in full-strength standard oocyte medium and measuring the swelling rate at 15 °C by video microscopy upon placement in a modified, isoosmotic Ringer's solution (190 mOsmol/kg) in which NaCl was replaced with boric acid by the approach of Wallace and Roberts[21] as described in ref 14. Under these assay conditions, the transport of boric acid into oocytes results in an inwardly directed osmotic gradient resulting in water uptake and oocyte swelling. The rate of solute uptake is reported as an oocyte swelling rate $[d(V/V_0)/min]$ determined by video microscopy as described above. Hg inhibition was assessed by incubation of the oocytes in Ringer's solution containing 1 mM $HgCl_2$ at room temperature for 10 min prior to the transport assay. Oocyte uptake assays using [^{3}H]glycerol and [^{14}C]urea were conducted as described in ref 21. Expression of the various aquaporin/MIPs in *Xenopus* oocytes was assessed by Western blotting with an anti-FLAG antibody as described in ref 21.

Total RNA Isolation and Quantitative Real-Time RT-PCR (Q-PCR). *A. thaliana* ecotype Columbia 0 seeds were germinated and grown under a long day cycle of light for 16 h and dark for 8 h at 22 °C as described in ref 24. Total RNA was isolated from tissue samples (200 mg) of 45-day-old *A. thaliana* plants, and first-strand cDNA synthesis and Q-PCR were conducted as described in ref 24. Q-PCR analysis was performed on an ABI Prism 7000 Sequence Detection System, and analysis was performed with the ABI Prism 7000 SDS software (PE Applied Biosystems, Foster City, CA). Gene-specific primers are listed in Table S1 of the Supporting Information. The *A. thaliana UBQ10* gene was used as an internal reference for standardization, and quantitation of *AtNIP7;1* expression was calculated using the comparative threshold cycle (Ct) method as described previously.[24]

Histochemical Methods. For the *AtNIP7;1*$_{pro}$*::GUS* reporter construct, a DNA fragment corresponding to 1085 bp of the *AtNIP7;1* gene upstream of the transcriptional start site was amplified by PCR using gene-specific primers (Table S1 of the Supporting Information) with *Bam*HI and *Eco*RI sites introduced for cloning into pCAMBIA1391Z[25] upstream of a promoterless

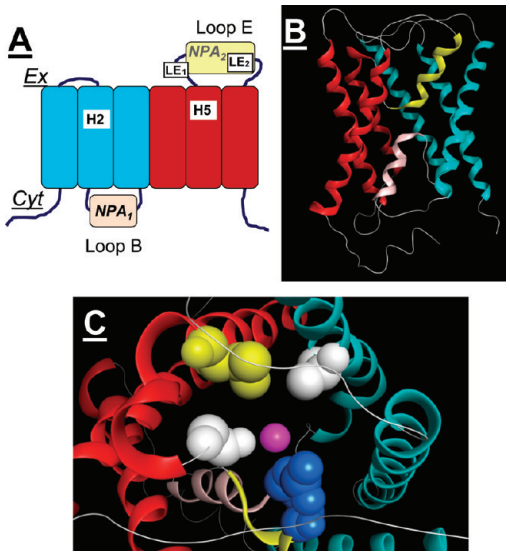

Figure 1. Homology model of AtNIP7;1. (A) Cartoon summarizing the topological features of the aquaporin/hourglass fold. The positions of the NPA boxes, a signature motif of aquaporins, in loop B and loop E are indicated. The four residues that form the aromatic arginine selectivity (ar/R) constriction are indicated using the position nomenclature (H2, H5, LE_1, and LE_2) described in ref 12. *Ex* indicates the extracellular side and *Cyt* the cytosolic side of the membrane. (B) Ribbon diagram of the AtNIP7;1 homology model constructed in MOE using the AQP0 (PDB entry 1YMG) structural template. The helix colors correspond to the positions of the transmembrane and NPA helices shown in panel A. The structure is viewed perpendicular to the axis of the transport pore with the extracellular side of the membrane at the top. (C) AtNIP7;1 model viewed down the transport pore axis from the extracellular face of the membrane with the side chains of the ar/R selectivity filter highlighted. The residues correspond to (in clockwise fashion starting from the top right) Ala85 (white) in the H2 position, Arg220 (blue) in the LE_2 position, Gly214 (white) in the LE_1 position, and Val205 (yellow) in the H5 position. The position of the transport substrate (in this case water) in the ar/R constriction based on the crystal structure[36] of the AQP0 template is denoted with a magenta sphere.

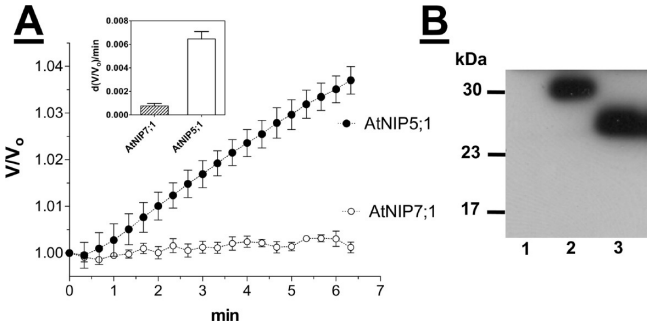

Figure 2. Boric acid transport activity of AtNIP7;1 in *Xenopus* oocytes. (A) Time course of boric acid-driven oocyte swelling of AtNIP5;1 and AtNIP7;1 cRNA-injected oocytes upon immersion in an isoosmotic Ringer's solution containing boric acid determined as described in Experimental Procedures. The swelling rates due to the uptake of boric acid followed by the osmotically driven uptake of water were measured by video microscopy. V/V_0 represents the increase in oocyte volume divided by the volume at time zero. The histogram in the inset shows the rate of boric acid-driven oocyte swelling corrected for basal transport through negative control (sterile water-injected) oocytes, with error bars showing the SEM (n = 5 oocytes). (B) Western blot of oocyte lysates (5 μg of protein/lane) with the anti-FLAG tag monoclonal antibody: lane 1, oocytes mock injected with sterile water; lane 2, AtNIP5;1-injected oocytes; lane 3, AtNIP7;1-injected oocytes. As expected, AtNIP5;1 (31.5 kDa) migrates at a higher-molecular mass position than AtNIP7;1 (28.8 kDa).

GUS reporter gene. *AtNIP7;1*$_{pro}$*::GUS* reporter constructs were transfected into *Agrobacterium tumefaciens* GV3101,[26] which was used for the transformation and generation of stable transgenic *A. thaliana* lines with the *AtNIP7;1*$_{pro}$*::GUS* reporter by using the floral dip method.[27] GUS staining and visualization were conducted on inflorescences of 6-week-old transgenic *A. thaliana* by the protocol described in ref 24.

For in situ hybridization, a 350 bp fragment of the *AtNIP7;1* gene was amplified from the *A. thaliana*'s flower cDNA sample using gene-specific primers (Table S1 of the Supporting Information). The PCR product was cloned into the pCR2.1-TOPO vector and was transformed into the TOP10 *E. coli* strain (Invitrogen, Carlsbad, CA). Digoxigenin (DIG)-labeled sense and antisense NIP7;1 RNA probes were prepared using the T7 RNA polymerase using DIG RNA labeling mix (Roche Diagnostics Corp., Indianapolis, IN) according to the manufacturer's instructions. For staining of floral tissues, young unopened flower buds of 6-week-old *A. thaliana* were fixed in 4% (w/v) paraformaldehyde in PBS (pH 7.5) and were embedded in paraffin. The tissue blocks were then sectioned to 10 μm thickness with a Sorvall JB-4A microtome equipped with a tungsten knife, and tissue sections were mounted on poly-L-lysine-coated glass slides. Samples were hybridized with the DIG-labeled NIP7;1 antisense (test) and sense (negative control) probes according to the manufacturer's protocol (Roche Diagnostics Corp.). The hybridization signal was detected by incubation with anti-DIG-alkaline phosphatase followed by colorimetirc staining with nitroblue tetrazolium/5-bromo-4-chloro-3-indolyl phosphate. Staining was observed and imaged using a Nikon ECLIPSE E600 microscope equipped with Micropublisher version 3.3 and QCapture version 2.60 (QImaging Corp., Burnaby, BC).

General Techniques. The sequences of all constructs generated were verified by automated DNA sequencing with a Perkin-Elmer Applied Biosystems 373 DNA sequencer at the University of Tennessee Molecular Biology Research Facility (Knoxville, TN).

RESULTS

Molecular Modeling and Functional Analyses of the AtNIP7;1 Protein. Alignment of the AtNIP7;1 protein sequence with various MIP structural templates revealed conservation of the key elements of the aquaporin fold (Figure S1 of the Supporting Information). AQP0, the template that is most structurally similar (37% identical sequence within the transmembrane and NPA helical areas), was used for homology modeling of AtNIP7;1 (Figure 1). The AtNIP7;1 homology model shows excellent superimposition with the AQP0 template (average carbon backbone rmsd of 0.7 Å), particularly of pore-forming residues, and allowed the placement of proposed ar/R residues (Figure S2 of the Supporting Information). The residues proposed to form the ar/R tetrad in AtNIP7;1 are Ala85 (H2), Val205 (H5), Gly214 (LE_1), and Arg220 (LE_2) (Figure 1). This ar/R signature, particularly the presence of alanine at the H2 position (NIP II-like) in place of a tryptophan (NIP I-like), is characteristic of the selectivity sequences of the NIP II boric acid transporters AtNIP5;1 and AtNIP6;1.[12,21]

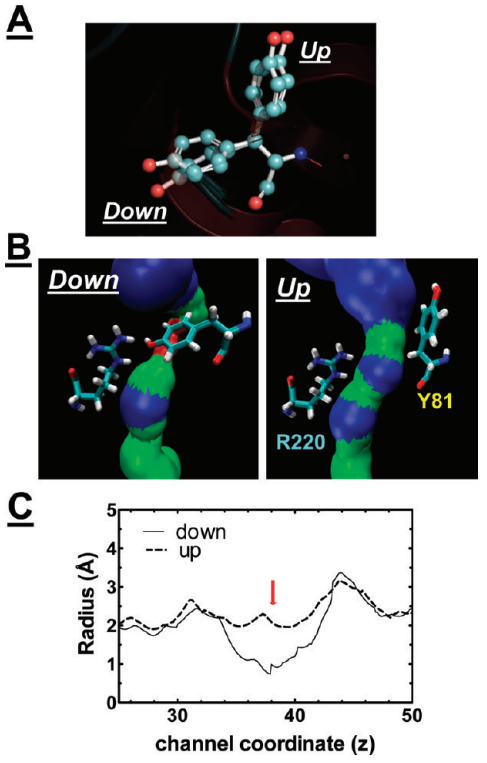

Figure 3. HOLE profiles of the AtNIP7;1 models. (A) Superimposition of homology models obtained for AtNIP7;1 viewed perpendicular to the transport pore axis with the Tyr81 side chain shown as a ball and stick representation. The two orientations of the Tyr81 phenolic side chain in either an *up* or *down* orientation relative to the pore axis are indicated. (B) Pore width of AtNIP7;1 in the *up* or *down* state analyzed by using HOLE. Surface representations are colored according to the pore width (blue for diameters of >5 Å, light green for >2 Å, and red for <2 Å). The side chains of Tyr81 in the *up* or *down* states relative to Arg220 are shown. (C) Pore radii of the Tyr81 *up* state (---) and *down* state (—), plotted along the *z* axis calculated with HOLE. The arrow shows the pore position of Tyr81.

To test whether AtNIP7;1 is functionally similar to these NIP II proteins, its permeability to boric acid was investigated upon expression in *Xenopus* oocytes (Figure 2). Comparison of AtNIP7;1- and AtNIP5;1-expressing oocytes shows that while both are expressed at equivalent levels, AtNIP7;1 shows a level of boric acid uptake reduced more than 10-fold compared to that of AtNIP5;1 (Figure 2), close to the rate of diffusion of boric acid through a lipid bilayer.

Further analysis of homology models provided a potential explanation for the lack of solute permeability exhibited by AtNIP7;1. This analysis revealed the presence of an unusual tyrosine (Tyr81) in transmembrane helix 2 that is located on the extracellular side of the H2 ar/R residue facing the pore and lying close to the Ar/R region in the three-dimensional structure (Figure S3 of the Supporting Information). Comparison of 10 separate AtNIP7;1 homology models generated by MOE showed excellent superimposition of the carbon backbone within the α-helical and pore-forming regions (rmsd ranging from 0.5 to 0.9 Å) but showed that the Tyr81 side chain can adopt two rotomer states that can be described as "*up*" or "*down*" with respect to the normal of the membrane plane (Figure 3). In the *down* configuration, the tyrosine appears to lie across the pore axis, suggesting that it may occlude the pore, while in the *up* configuration, the side chain points up to the extracellular vestibule, almost parallel to the channel, suggesting that it may open the pore. This was tested by analysis of the two representative AtNIP7;1 models with the *up* or *down* configuration of Tyr81 by using HOLE. The *up* state shows an open pore characteristic of other NIP II proteins,[12,21] but the *down* state shows a pinched pore with a diameter of <2 Å (Figure 3). This suggests that AtNIP7;1 could potentially exist in either an open or closed state, raising the possibility that transport through this channel may be determined by the position of the Tyr81 side chain. In comparison, modeling of the AtNIP5;1 and AtNIP6;1 boric acid transport channels shows the presence of an Asn or a Cys residue at the corresponding position of Tyr81 in AtNIP 7;1 (Figure S3 of the Supporting Information). As a result, the predicted pore apertures of AtNIP5;1 and AtNIP6;1 are open compared to that of AtNIP7;1 (Figure S3 of the Supporting Information).

To test the hypothesis that Tyr81 may regulate AtNIP7;1 transport, site-directed mutagenesis of Tyr81 to the smaller Cys residue (AtNIP7;1 Y81C) was conducted, and boric acid uptake assays were performed. Substitution of Y81 with cysteine resulted in a robust level of boric acid transport that was 20-fold higher than that of wild-type AtNIP7;1 and 4-fold higher than that of the positive control AtNIP5;1 boric acid facilitator (Figure 4). In addition, pretreatment of AtNIP7;1 Y81C-injected oocytes with the channel blocker $HgCl_2$ resulted in a 70% reduction of the boric acid transport activity (Figure 4C), suggesting the proximity of this residue to the transport pore as predicted by molecular modeling (Figure S3 of the Supporting Information).

While an increase in the boric acid uptake rate was observed for the AtNIP7;1 Y81C mutant, the osmotic water permeabilities (P_f) of both AtNIP7;1- and AtNIP7;1 Y81C-injected oocytes were indistinguishable from those of the negative control oocytes (Figure 5). In addition to transport of the physiologically relevant solute boric acid, NIP II protein also exhibits the ability to transport test substrates glycerol and urea,[21] which are useful for the direct analysis of transport using radiolabeled solute uptake assays. Analysis of the AtNIP7;1 Y81C mutant shows that substitution of an AtNIP6;1-like cysteine results in the opening of the pore to transport of glycerol as well as urea (Figure 6), consistent with previous analyses of AtNIP6;1.[21] Thus, similar to other NIP II channels,[14] opening of the AtNIP7;1 pore results in boric acid transport, as well as permeation by urea and glycerol test solutes, but the protein remains impermeable to water without detectable aquaporin activity.

Molecular Dynamics Simulation of the Tyr81−Arg220 Interaction. To gain insight into how the *down* configuration of Tyr81 might be stabilized, a 5 ns molecular dynamics simulation was performed on the AtNIP7;1 model (Figure 7). During the molecular dynamics simulation, rotation of the Arg220 side chain in the ar/R region was observed with the guanidinium moiety moving within hydrogen bonding distance of the Tyr81 hydroxyl present in the *down* configuration. HOLE modeling shows that the formation of this hydrogen bond would effectively close the AtNIP7;1 channel (Figure 7). This observation suggests that hydrogen bond interaction of the Tyr81 hydroxyl group with the Arg220 side chain could stabilize the *down* state of the Tyr81, resulting in a low-energy closed state. To test this hypothesis, site-directed mutagenesis of AtNIP7;1 to generate a Phe81 substitution (AtNIP7;1 Y81F) was performed. Expression of AtNIP7;1 Y81F in *Xenopus* oocytes resulted in an increase in the boric acid transport rate compared to that of AtNIP7;1

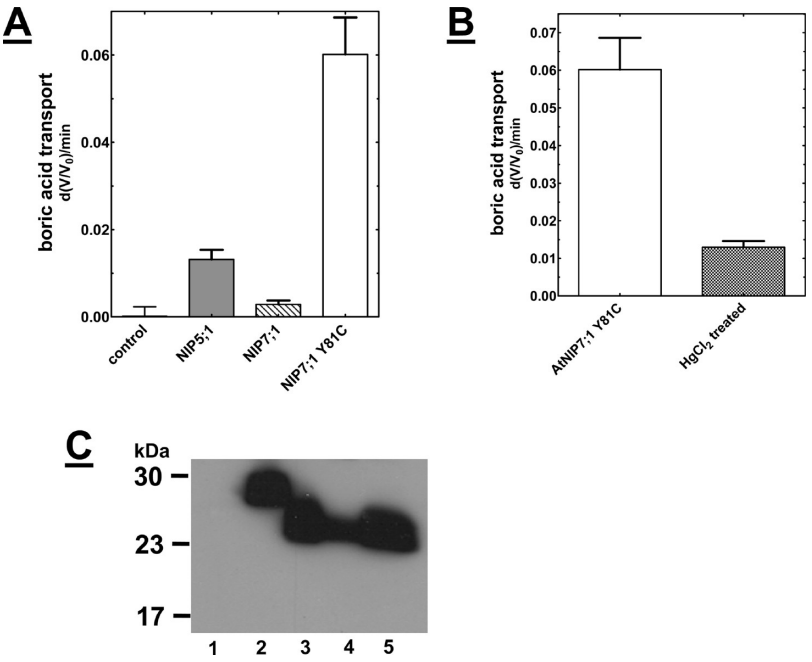

Figure 4. Boric acid transport activity of AtNIP7;1 Y81C in *Xenopus* oocytes. (A) Boric acid transport rates of AtNIP5;1, AtNIP7;1, and AtNIP7;1 Y81C cRNA-injected oocytes, as well as negative control oocytes, determined by same approach shown in Figure 2. The error bars show the SEM ($n = 9$ oocytes). (B) Sensitivity of the boric acid permeability of AtNIP7;1 Y81C-injected oocytes to $HgCl_2$ (1 mM). The error bars show the SEM ($n = 9$ oocytes for control and AtNIP7;1 Y81C; $n = 7$ oocytes for AtNIP7;1 Y81C treated with $HgCl_2$). (C) Western blot of oocyte lysates (5 μg of protein/lane) with the anti-FLAG tag monoclonal antibody: lane 1, negative control oocytes; lane 2, AtNIP5;1-injected oocytes; lane 3, AtNIP7;1-injected oocytes; lane 4, AtNIP7;1 Y81C-injected oocytes; lane 5, AtNIP7;1 Y81C-injected oocytes incubated with 1 mM $HgCl_2$.

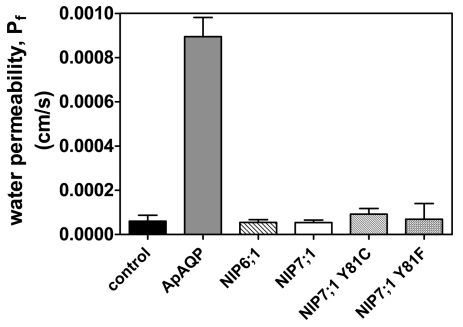

Figure 5. Osmotic water peremeabilities of AtNIP7;1-expressing oocytes. Oocytes were injected with the indicated cRNAs or with sterile water (negative control). The osmotic water permeability (P_f) was determined from the rate of oocyte swelling upon incubation in a hypoosmotic Ringer's solution as described in Experimental Procedures. The error bars show the SEM ($n = 8$ oocytes). ApAQP[22] was used as a positive control aquaporin cRNA.

(Figure 8). The transport of boric acid through AtNIP7;1 Y81F was still approximately 3-fold slower than that observed with AtNIP7;1 Y81C, suggesting that while the Phe substitution results in channel opening, it still restricted boric acid permeability compared to substitution with a smaller Cys residue. Nevertheless, the rate of transport of boric acid through AtNIP7;1 Y81F was significantly higher than that of AtNIP6;1, which is an established boric acid transporter of *A. thaliana*.[14]

AtNIP7;1 Is Expressed in Developing Pollen in Young Anthers. AtNIP5;1 (roots) and AtNIP6;1 (leaf nodes) show organ-specific expression in *A. thaliana* that is correlated with distinct boric acid transport functions in these tissues.[15] The tissue versus organ distribution of the *AtNIP7;1* transcript in 6-week-old, flowering *A. thaliana* plants was investigated by Q-PCR analysis and was standardized to the constitutive *UBQ10* transcript (Figure 9A). The results show predominant expression of *AtNIP7;1* in reproductive tissue (flowers and siliques) with the highest expression levels (>50-fold over the basal expression level in leaves) observed in flowers. Investigation of tissue-specific expression in 45-day-old inflorescences in *AtNIP7;1*$_{pro}$*::GUS* reporter transgenic *A. thaliana* plants shows *GUS* expression principally in young unopened floral buds with the GUS signal declining in opened, more mature floral organs (Figure 9B). Within young flowers, expression is specific for anther tissues (Figure 9B).

To investigate the cellular localization of *AtNIP7;1* expression in developing anthers, in situ hybridization was performed with a *AtNIP7;1*-specific probe. The results showed detection of *AtNIP7;1* in developing pollen microspores of early floral buds with antisense *AtNIP7;1* probe hybridization (Figure 9C). Specificity is apparent because hybridization with the sense *AtNIP7;1* probe showed no apparent signal. The results suggest that *AtNIP7;1* is a flower-enhanced transcript that is selectively expressed in developing pollen grains in young anther tissues.

DISCUSSION

The diversification of members of the aquaporin superfamily during land plant evolution has led to the generation of a specialized subclass of channels, the nodulin 26-like intrinsic proteins, which have acquired additional transport selectivities.[3,15,28,29] Analysis of NIPs across several plant genomes has led to classification into "pore subclasses" based on the proposed structure of the ar/R pore selectivity filter. "NIP I"

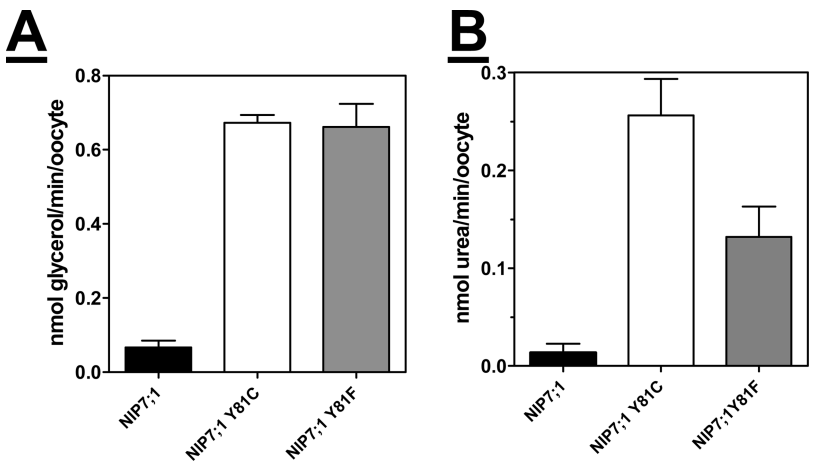

Figure 6. Urea and glycerol peremeabilities of AtNIP7;1-expressing oocytes. Oocytes were injected with the indicated cRNAs or with sterile water (negative control). (A) The [^{3}H]glycerol permeability or (B) [^{14}C]urea permeability of the indicated oocytes were determined as described in ref 21. The error bars show the SEM (n = 4).

proteins are similar to the family archetype, soybean nodulin 26, and possess a canonical ar/R sequence (H2, Trp; H5, Val; LE_1, Ala or Gly; LE_2, Arg).[12] NIP I proteins form aquaglyceroporin channels.[29] "NIP II" proteins adopt distinct ar/R pore selectivity structures (H2, Ala, Gly, or Thr; H5, Ile or Val; LE_1, Gly or Ala; LE_2, Arg) and show permeabilty to solutes larger than those allowed by NIP I proteins.[21] The biological substrate for NIP II proteins is boric acid,[15] although analysis in oocytes shows that they are also permeated by urea and glycerol test solutes.[21] More recently, a third group, the "NIP III" proteins, that are specific to Si-accumulating plants such as rice has been identified.[30−32] These proteins form metalloid transport channels that facilitate the uptake and transport of silicic acid[33] through a specialized ar/R filter (H2, Gly; H5, Ser; LE_1, Gly; LE_2, Arg).

A. thaliana, which does not accumulate Si, does not contain genes encoding NIP III proteins. However, *A. thaliana* does possess three NIP II genes: *AtNIP5;1*, *AtNIP6;1*, and *AtNIP7;1*. AtNIP5;1 and AtNIP6;1 proteins have been established as boric acid channels that are expressed within root tissues and leaf nodal regions, respectively, and play critical roles in the uptake of B.[13,14] In this study, we show that *AtNIP7;1* is predominantly expressed in developing pollen grains of young floral buds and encodes a protein that possesses boric acid transport activity. However, unlike the AtNIP5;1 and AtNIP6;1 channels, which show constitutive boric acid transport activity,[13,14] the AtNIP7;1 channel shows unusual transport properties that are the result of a tyrosine residue (Tyr81) located on helix 2, approximately one α-helical turn on the extracellular side of the ar/R selectivity filter. Two potential rotomeric states of Tyr81 are observed in AtNIP7;1 pore models, with MD suggesting stabilization of the Tyr81 side chain in the *down* configuration by Arg220, resulting in closure of the channel (predicted pore aperture of <1 Å). Support for a closed state of the channel comes from observations that expression of AtNIP7;1 in *Xenopus* oocytes results in normal expression of the protein but little measurable transport activity over negative control oocytes. Intrinsically low boric acid transport activity observed for wild-type AtNIP7;1 is supported by previous observations of metalloid sensitivity in yeast.[34,35] The toxic metalloid compound $As(OH)_3$ is a structural analogue of boric acid and has been used in yeast expression experiments to infer the relative transport activities of various NIPs. Compared to AtNIP5;1 and AtNIP6;1, AtNIP7;1 provided only modest sensitivity to the growth of yeast on $As(OH)_3$, suggesting a lower transport activity.[34,35]

The two boric acid transporters from *A. thaliana*, AtNIP5;1 and AtNIP6;1, possess an Asn and a Cys, respectively, which are predicted to remove the potential pore blocking properties associated with the bulkier Tyr (Figure S3 of the Supporting Information). Substitution of a Cys residue for Tyr81 completely opens the channel to boric acid transport, at a rate higher than that of the established NIP boric acid channels. Inhibition of this transport by Hg^{2+} suggests that this cysteine side chain lies close to the pore as predicted in structural models. Interestingly, AtNIP7;1 Y81C shows no apparent transport of water. This suggests that, similar to AtNIP6;1,[14] AtNIP7;1 in an open configuration forms a water-tight boric acid channel.

The observation of two rotomeric states of Tyr81 in AtNIP7;1 is consistent with the "pore pinching" gating properties observed for certain aquaporins based on structural analyses.[36−41] The idea of the conserved ar/R arginine serving a role as a potential gate in aquaporins was suggested on the basis of MD simulations and structural analyses of the water-specific *E. coli* AQP Z channel.[39,42,43] Wang et al.[43] observed a thermodynamic equilibrium of the ar/R Arg189 of AQP Z between two discrete rotameric states: an *up* state, characteristic of most aquaporin structures, in which the Arg side chain is oriented toward the periplasmic side of the pore parallel to the pore axis, and a *down* state, in which the Arg side chain lies across the pore. Subsequent determination of the AQP Z structure[39] showed that Arg189 within monomers in each tetrameric structure adopts either an *up* or *down* configuration, presumably because of crystal packing forces. Movement of Arg189 into the *down* configuration is stabilized by a hydrogen bond with the carbonyl backbone of Thr183 (another ar/R water ligand) that results in the loss of water from the selectivity region and a "closed" channel state.[39] The proposal of this thermal fluctuation between rotomeric states serving as a gate for water transport was advanced.[39,43]

In the present study, it is proposed that AtNIP7;1 adopts a similar pore regulatory mechanism on the basis of MD simulations that show movement of the ar/R Arg220 guanidinium group into a *down* configuration similar to that observed in AQP Z. On the

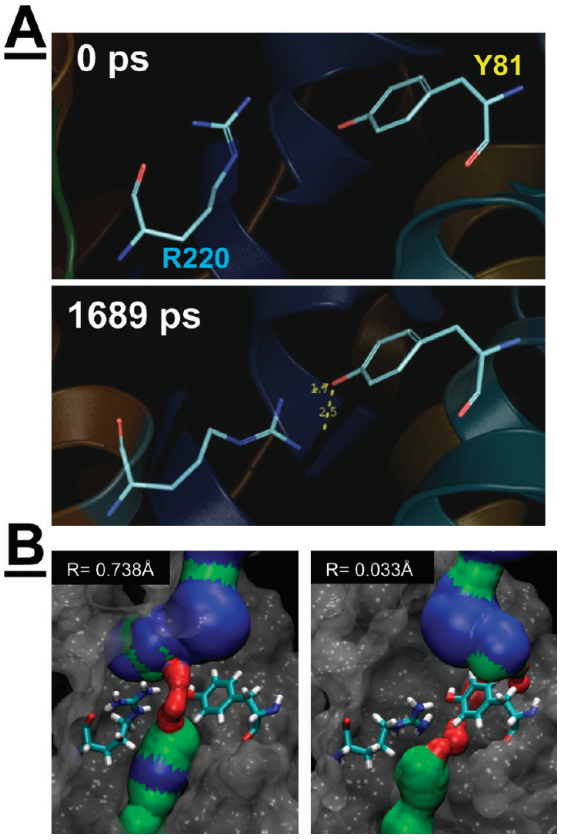

Figure 7. Predicted interaction of Tyr81 and Arg220 by molecular dynamics simulation. (A) Molecular dynamics simulation of an AtNIP7;1 model with the Tyr81 side chain in the *down* position performed as described in Experimental Procedures. The top panel shows a side view of the AtNIP7;1 pore at the beginning of the simulation, showing the positions of the Arg220 and Tyr81 side chains. The bottom panel shows the same view at 1689 ps showing the reorientation of the Arg220 side chain in a configuration perpendicular to the pore axis, stabilized by a hydrogen bond (yellow dotted line) formed between the guanidinium group (blue) of Arg220 and the phenolic OH group (red) of Tyr81. (B) HOLE depiction of the ar/R pore region at the beginning of the simulation (left) and at the end of the simulation (right) with the radius of the ar/R aperture indicated numerically on each panel. Residues are shown in surface representation except for the Arg220 and Tyr81 side chains, which are shown as sticks.

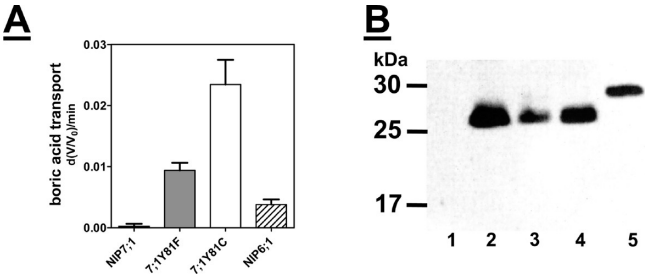

Figure 8. Effect of removal of the tyrosine 81 hydroxyl group on the boric acid transport of AtNIP7;1. (A) Comparison of the boric acid transport rates of oocytes injected with the indicated cRNAs corresponding to wild-type AtNIP7;1 or its site-directed mutants. AtNIP6;1[14] represents a positive control boric acid transporter. The error bars represent the SEM (n = 7 or 8 oocytes per cRNA). (B) Western blot of oocyte lysates (5 μg of protein/lane) with the anti-FLAG tag monoclonal antibody: lane 1, uninjected oocytes; lane 2, AtNIP7;1-injected oocytes; lane 3, AtNIP7;1 Y81C-injected oocytes; lane 4, AtNIP7;1 Y81F-injected oocytes; lane 5, AtNIP6;1-injected oocytes.

basis of the orientation of the Tyr81 and Arg220 side chains, it is proposed that hydrogen bond interactions between the Tyr phenolic hydroxyl group and the Arg guanidinium group could contribute to stabilization of the closed orientation. In support of this hypothesis, removal of the Tyr81 hydroxyl group by mutagenesis to Phe results in channel opening.

Comparison of a number of NIP II proteins across several plant species suggests that the helix 2 position occupied by Tyr81 in AtNIP7;1 is either a Tyr, Asn, or Cys (Figure S4 of the Supporting Information). The finding of NIP II homologues in other plant species with a Tyr residue at this position suggests that the presence of this potential gating residue may be conserved in other metalloid transporters in plants. Why would AtNIP7;1 transporters require this type of regulation? A potential clue comes from the dual effects of boric acid on plant tissues.[15,44−46] Boron is an essential plant nutrient that is necessary for the formation of borate−diol ester cross-links in dimers of the plant pectic polysaccharide rhamnogalacturonan II.[16] This cross-link is necessary for the mechanical stability of the primary cell wall essential for normal plant growth and development. However, at high concentrations, boron is toxic to plant growth.[44,46] As a result, plants have developed sophisticated transcriptional and posttranscriptional mechanisms for the regulation of the expression and subcellular localization of NIP and BOR boric acid transporters to maintain an optimal homeostasis to satisfy boron nutritional needs while preventing toxicity.[15,45] The presence of an intrinsic gate within the boric acid transport pore would provide an additional, and more rapid, regulatory mechanism. Less clear at present is the nature of the signals or environmental cues that would regulate this potential gating mechanism. On the basis of analogy to other aquaporins,[36−41] potential regulators of transport gating could be pH, protein phosphorylation, and protein−protein interaction. With respect to protein phosphorylation, it is interesting to note that NIP II proteins, including AtNIP7;1, have conserved MAP kinase phosphorylation motifs within their N- and C-terminal domains,[29,34] and phosphorylation of these regions by recombinant MAP kinases has been observed in vitro.[29]

GUS promoter expression analyses of *AtNIP7;1* in *A. thaliana* inflorescences show preferential expression in the anthers of young unopened floral buds. *A. thaliana* flower development is divided into 20 stages that represent a series of landmark events beginning with flower initiation and ending with seed fall.[47] Analysis of *AtNIP7;1* on floral developmental microarrays shows high levels of the transcript at stage 9 and then a gradual decline over flower stages 10−12 with little expression observed at stage 15, which occurs after flower opening and dehiscence (Figure S5A of the Supporting Information).

In a previous study of the effects of boron limitation on anther development in wheat, Huang et al.[48] identified two particularly sensitive developmental stages. The most sensitive stage is meiosis of the pollen mother cells to produce tetrad microspores. In *A. thaliana*, this would correspond with floral stage 9,[47,49] which correlates with the highest level of expression of *AtNIP7;1*. A secondary period of boron sensitivity is the period spanning pollen mitosis I and II during pollen grain maturation.[48] This occurs during flower stages 11 and 12. Microarray data from developing *A.thaliana* pollen at these stages show that AtNIP7;1 is induced in anthers after mitosis I and accumulates at a peak level

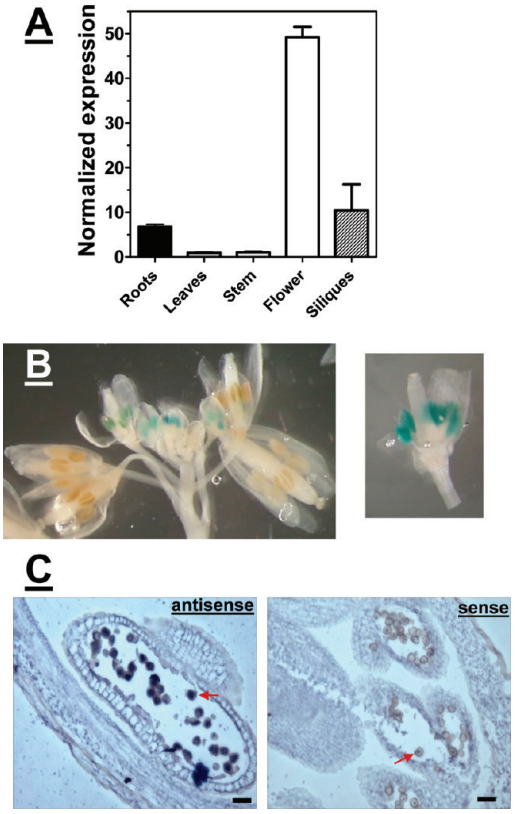

Figure 9. Selective expression of *AtNIP7;1* in *A. thaliana* in anthers of developing flowers. (A) Q-PCR analysis for *AtNIP7;1* expression in dissected organs of 45-day-old *A. thaliana* plants. Data were normalized to *AtNIP7;1* expression in leaf tissues. Error bars show the SEM of three (siliques), five (stems), or six (flowers, leaves, and roots) biological replicates. (B) Analysis of GUS expression in inflorescences of 6-week-old transgenic *A. thaliana* plants expressing the $AtNIP7;1_{pro}$:*GUS* reporter construct. The right panel shows a dissected stage 11 flower showing GUS expression in anthers. (C) In situ hybridization analysis of *AtNIP7;1* expression in anther sections of unopened *A. thaliana* flower buds (stage 11). Tissue sections were hybridized with an *AtNIP7;1* antisense probe (left) and an *AtNIP7;1* sense probe (right) as described in Experimental Procedures. Each tissue section was counterstained with Eosin Y for contrast. Size bars are 20 μm. Arrows denote pollen microspores.

at mitosis II (Figure S5B of the Supporting Information). Overall, the data suggest that AtNIP7;1 may play a role as a regulated boric acid transporter during boron-dependent developmental stages of the male gametophyte in *A. thaliana*. Further investigation, including the analysis of *AtNIP7;1* knockout *A. thaliana* mutants, will help elucidate the precise role of this flower-specific NIP channel in floral development.

■ ASSOCIATED CONTENT

Ⓢ Supporting Information. Sequence and structure alignments of AtNIP7;1 with aquaporin crystal structure templates (Figures S1 and S2), comparative modeling of the pore selectivity regions of the NIP II subfamily proteins of *Arabidopsis* (Figure S3), sequence comparison of helix II of plant NIP II proteins (Figure S4), AtNIP7;1 transcript levels during floral and pollen development (Figure S5), and a list of oligonucleotide primers used in this study (Table S1). This material is available free of charge via the Internet at http://pubs.acs.org.

■ AUTHOR INFORMATION

Corresponding Author

*Department of Biochemistry and Cellular and Molecular Biology, 133 Hesler Biology Bldg., The University of Tennessee, Knoxville, TN 37996. Telephone: (865) 974-4070. Fax: (865) 974-6306. E-mail: drobert2@utk.edu.

Funding Sources

Supported by National Science Foundation Grants MCB-0618075 and MCB-1121465.

■ ABBREVIATIONS

AQP, aquaporin; ar/R, aromatic arginine; DIG, digoxigenin; GUS, β-glucuronidase; MIP, major instrinsic protein; MOE, Molecular Operating Environment; NIP, nodulin 26-like intrinsic protein; PCR, polymerase chain reaction; Q-PCR, real-time quantitative PCR; SEM, standard error of the mean.

■ REFERENCES

(1) Gomes, D., Agasse, A., Thiebaud, P., Delrot, S., Geros, H., and Chaumont, F. (2009) Aquaporins are multifunctional water and solute transporters highly divergent in living organisms. *Biochim. Biophys. Acta 1788*, 1213–1228.

(2) King, L. S., Kozono, D., and Agre, P. (2004) From structure to disease: The evolving tale of aquaporin biology. *Nat. Rev. Mol. Cell Biol. 5*, 687–698.

(3) Ludewig, U., and Dynowski, M. (2009) Plant aquaporin selectivity: Where transport assays, computer simulations and physiology meet. *Cell. Mol. Life Sci. 66*, 3161–3175.

(4) Maurel, C., Verdoucq, L., Luu, D. T., and Santoni, V. (2008) Plant aquaporins: Membrane channels with multiple integrated functions. *Annu. Rev. Plant Biol. 59*, 595–624.

(5) Walz, T., Fujiyoshi, Y., and Engel, A. (2009) The AQP structure and functional implications. *Handb. Exp. Pharmacol. 190*, 31–56.

(6) de Groot, B. L., and Grubmuller, H. (2001) Water permeation across biological membranes: Mechanism and dynamics of aquaporin-1 and GlpF. *Science 294*, 2353–2357.

(7) Danielson, J. A., and Johanson, U. (2008) Unexpected complexity of the aquaporin gene family in the moss *Physcomitrella patens*. *BMC Plant Biol. 8*, 45.

(8) Gupta, A. B., and Sankararamakrishnan, R. (2009) Genome-wide analysis of major intrinsic proteins in the tree plant *Populus trichocarpa*: Characterization of XIP subfamily of aquaporins from evolutionary perspective. *BMC Plant Biol. 9*, 134.

(9) Johanson, U., Karlsson, M., Johansson, I., Gustavsson, S., Sjövall, S., Fraysse, L., Weig, A., and Kjellbom, P. (2001) The complete set of genes encoding major intrinsic proteins in *Arabidopsis* provides a framework for a new nomenclature for major intrinsic proteins in plants. *Plant Physiol. 126*, 1358–1369.

(10) Quigley, F., Rosenberg, J., Shachar-Hill, Y., and Bohnert, H. (2002) From genome to function: The *Arabidopsis* aquaporins. *Genome Biol. 3*, research0001.1–research0001.17.

(11) Sakurai, J., Ishikawa, F., Yamaguchi, T., Uemura, M., and Maeshima, M. (2005) Identification of 33 rice aquaporin genes and analysis of their expression and function. *Plant Cell Physiol. 46* 1568–1577.

(12) Wallace, I. S., and Roberts, D. M. (2004) Homology modeling of representative subfamilies of *Arabidopsis* major intrinsic proteins. Classification based on the aromatic/arginine selectivity filter. *Plant Physiol. 135*, 1059–1068.

(13) Takano, J., Wada, M., Ludewig, U., Schaaf, G., von Wiren, N., and Fujiwara, T. (2006) The *Arabidopsis* major intrinsic protein NIP5;1 is essential for efficient boron uptake and plant development under boron limitation. *Plant Cell 18*, 1498–1509.

(14) Tanaka, M., Wallace, I. S., Takano, J., Roberts, D. M., and Fujiwara, T. (2008) NIP6;1 is a boric acid channel for preferential transport of boron to growing shoot tissues in *Arabidopsis*. *Plant Cell 20*, 2860–2875.

(15) Takano, J., Miwa, K., and Fujiwara, T. (2008) Boron transport mechanisms: Collaboration of channels and transporters. *Trends Plant Sci. 13*, 451–457.

(16) O'Neill, M. A., Ishii, T., Albersheim, P., and Darvill, A. G. (2004) Rhamnogalacturonan II: Structure and function of a borate cross-linked cell wall pectic polysaccharide. *Annu. Rev. Plant Biol. 55* 109–139.

(17) Gorelick, D., Praetorius, J., Tsunenari, T., Nielsen, S., and Agre, P. (2006) Aquaporin-11: A channel protein lacking apparent transport function expressed in brain. *BMC Biochem. 7*, 14.

(18) Heymann, J. B., and Engel, A. (2000) Structural clues in the sequences of the aquaporins. *J. Mol. Biol. 295*, 1039–1053.

(19) Foloppe, N., and MacKerell, A. D., Jr. (2000) All-atom empirical force field for nucleic acids: (1) Parameter optimization based on small molecule and condensed phase macromolecular target data. *J. Comput. Chem. 21*, 86–104.

(20) Smart, O. S., Breed, J., Smith, G. R., and Sansom, M. S. (1997) A novel method for structure-based prediction of ion channel conductance properties. *Biophys. J. 72*, 1109–1126.

(21) Wallace, I. S., and Roberts, D. M. (2005) Distinct transport selectivity of two structural subclasses of the nodulin-like intrinsic protein family of plant aquaglyceroporin channels. *Biochemistry 44* 16826–16834.

(22) Shakesby, A. J., Wallace, I. S., Isaacs, H. V., Pritchard, J., Roberts, D. M., and Douglas, A. E. (2009) A water-specific aquaporin involved in aphid osmoregulation. *Insect Biochem. Mol. Biol. 39*, 1–10.

(23) Rivers, R., Dean, R., Chandy, G., Hall, J., Roberts, D., and Zeidel, M. (1997) Functional analysis of nodulin 26, an aquaporin in soybean root nodule symbiosomes. *J. Biol. Chem. 272*, 16256–16261.

(24) Choi, W., and Roberts, D. (2007) Arabidopsis NIP2;1, a major intrinsic protein transporter of lactic acid induced by anoxic stress. *J. Biol. Chem. 282*, 24209–24218.

(25) Hajdukiewicz, P., Svab, Z., and Maliga, P. (1994) The small, versatile pPZP family of *Agrobacterium* binary vectors for plant transformation. *Plant Mol. Biol. 25*, 989–994.

(26) Koncz, C., and Schell, J. (1986) The Promoter of Tl-DNA Gene 5 Controls the Tissue-Specific Expression of Chimeric Genes Carried by a Novel Type of Agrobacterium Binary Vector. *Mol. Gen. Genet. 204*, 383–396.

(27) Clough, S. J., and Bent, A. F. (1998) Floral dip: A simplified method for *Agrobacterium*-mediated transformation of *Arabidopsis thaliana*. *Plant J. 16*, 735–743.

(28) Ma, J. F., and Yamaji, N. (2006) Silicon uptake and accumulation in higher plants. *Trends Plant Sci. 11*, 392–397.

(29) Wallace, I. S., Choi, W. G., and Roberts, D. M. (2006) The structure, function and regulation of the nodulin 26-like intrinsic protein family of plant aquaglyceroporins. *Biochim. Biophys. Acta 1758* 1165–1175.

(30) Liu, Q., Wang, H., Zhang, Z., Wu, J., Feng, Y., and Zhu, Z. (2009) Divergence in function and expression of the NOD26-like intrinsic proteins in plants. *BMC Genomics 10*, 313.

(31) Mitani, N., Yamaji, N., and Ma, J. F. (2008) Characterization of substrate specificity of a rice silicon transporter, Lsi1. *Pfluegers Arch. 456*, 679–686.

(32) Rouge, P., and Barre, A. (2008) A molecular modeling approach defines a new group of Nodulin 26-like aquaporins in plants. *Biochem. Biophys. Res. Commun. 367*, 60–66.

(33) Ma, J. F., Tamai, K., Yamaji, N., Mitani, N., Konishi, S., Katsuhara, M., Ishiguro, M., Murata, Y., and Yano, M. (2006) A silicon transporter in rice. *Nature 440*, 688–691.

(34) Bienert, G. P., Thorsen, M., Schussler, M. D., Nilsson, H. R., Wagner, A., Tamas, M. J., and Jahn, T. P. (2008) A subgroup of plant aquaporins facilitate the bi-directional diffusion of $As(OH)_3$ and $Sb(OH)_3$ across membranes. *BMC Biol. 6*, 26.

(35) Isayenkov, S. V., and Maathuis, F. J. (2008) The *Arabidopsis thaliana* aquaglyceroporin AtNIP7;1 is a pathway for arsenite uptake. *FEBS Lett. 582*, 1625–1628.

(36) Gonen, T., Sliz, P., Kistler, J., Cheng, Y., and Walz, T. (2004) Aquaporin-0 membrane junctions reveal the structure of a closed water pore. *Nature 429*, 193–197.

(37) Harries, W., Akhavan, D., Miercke, L., Khademi, S., and Stroud, R. (2004) The channel architecture of aquaporin 0 at a 2.2-Å resolution. *Proc. Natl. Acad. Sci. U.S.A. 101*, 14045–14050.

(38) Hedfalk, K., Tornroth-Horsefield, S., Nyblom, M., Johanson, U., Kjellbom, P., and Neutze, R. (2006) Aquaporin gating. *Curr. Opin. Struct. Biol. 16*, 447–456.

(39) Jiang, J., Daniels, B. V., and Fu, D. (2006) Crystal structure of AqpZ tetramer reveals two distinct Arg-189 conformations associated with water permeation through the narrowest constriction of the water-conducting channel. *J. Biol. Chem. 281*, 454–460.

(40) Tornroth-Horsefield, S., Hedfalk, K., Fischer, G., Lindkvist-Petersson, K., and Neutze, R. (2010) Structural insights into eukaryotic aquaporin regulation. *FEBS Lett. 584*, 2580–2588.

(41) Tornroth-Horsefield, S., Wang, Y., Hedfalk, K., Johanson, U., Karlsson, M., Tajkhorshid, E., Neutze, R., and Kjellbom, P. (2006) Structural mechanism of plant aquaporin gating. *Nature 439*, 688–694.

(42) Savage, D. F., Egea, P. F., Robles-Colmenares, Y., O'Connell, J. D., III, and Stroud, R. M. (2003) Architecture and selectivity in aquaporins: 2.5 Å X-ray structure of aquaporin Z. *PLoS Biol. 1*, e72.

(43) Wang, Y., Schulten, K., and Tajkhorshid, E. (2005) What makes an aquaporin a glycerol channel? A comparative study of AqpZ and GlpF. *Structure 13*, 1107–1118.

(44) Camacho-Cristobal, J. J., Rexach, J., and Gonzalez-Fontes, A. (2008) Boron in plants: Deficiency and toxicity. *J. Integr. Plant Biol. 50*, 1247–1255.

(45) Miwa, K., Kamiya, T., and Fujiwara, T. (2009) Homeostasis of the structurally important micronutrients, B and Si. *Curr. Opin. Plant Biol. 12*, 307–311.

(46) Nable, R. O., Banuelos, G. S., and Paull, J. G. (1997) Boron toxicity. *Plant Soil 193*, 181–198.

(47) Smyth, D. R., Bowman, J. L., and Meyerowitz, E. M. (1990) Early flower development in *Arabidopsis*. *Plant Cell 2*, 755–767.

(48) Huang, L. B., Pant, J., Dell, B., and Bell, R. W. (2000) Effects of boron deficiency on anther development and floret fertility in wheat (*Triticum aestivum* L-'Wilgoyne'). *Ann. Bot. 85*, 493–500.

(49) Sanders, P. M., Bui, A. Q., Weterings, K., McIntire, K. N., Hsu, Y. C., Lee, P. Y., Truong, M. T., Beals, T. P., and Goldberg, R. B. (1999) Anther developmental defects in *Arabidopsis thaliana* male-sterile mutants. *Sex. Plant Reprod. 11*, 297–322.